AEM
Journals.ASM.org

An Unbiased Method for Clustering Bacterial Effectors Using Host Cellular Phenotypes

Andrea J. Dowling, David J. Hodgson

Biosciences, College of Life & Environmental Sciences, University of Exeter, Cornwall Campus, Penryn, United Kingdom

We present a novel method implementing unbiased high-content morphometric cell analysis to classify bacterial effector phenotypes. This clustering methodology represents a significant advance over more qualitative visual approaches and can also be used to classify, and therefore predict the likely function of, unknown effector genes from any microbial genome. As a proof of concept, we use this approach to investigate 23 genetic regions predicted to encode antimacrophage effectors located across the genome of the insect and human pathogen *Photorhabdus asymbiotica*. Statistical cluster analysis using multiple cellular measures categorized treated macrophage phenotypes into three major groups relating to their putative functionality: (i) adhesins, (ii) cytolethal toxins, and (iii) cytomodulating toxins. Further investigation into their effects on phagocytosis revealed that several effectors also modulate this function and that the nature of this modulation (increased or decreased phagocytosis) is linked to the phenotype cluster group. Categorizing potential functionalities in this way allows rapid functional follow-up of key candidates for more-directed cell biological or biochemical investigation. Such an unbiased approach to the classification of candidate effectors will be useful for describing virulence-related regions in a wide range of genomes and will be useful in assigning putative functions to the growing number of microbial genes whose function remains unclear from homology searching.

Qualitative visual analysis of bacterial effector interaction with host cells provides essential insights necessary for understanding effector functions. Manual inspection and quantification of image data are subjective and open to inaccuracy and, further, are prohibitively time-consuming for large data sets. Unbiased numeric quantification is important in order to statistically validate different phenotypes (1). Here, we describe a novel morphological analysis method to functionally group bacterial effectors on a genomic scale. By using a combination of specifically developed, unbiased, high-content cellular analysis, bioinformatics, and statistics, we classify regions of interest (ROI) in the genome of a bacterial pathogen based on the morphological alterations that they induce in macrophages using multiple cellular measures.

To illustrate this approach, we use candidate effectors from *Photorhabdus asymbiotica*, an insect and human pathogen whose infection biology is largely uncharacterized (2, 3). The genome of strain ATCC 43949, isolated from a human infection in North America, has now been completed (4). *P. asymbiotica* has so far been described as a facultative intracellular pathogen with the ability to cause cell death via apoptosis in mammalian macrophage-like cells (5). The ability of a pathogen to manipulate immune cells, such as macrophages, is critical in the establishment of successful infection, as these phagocytes are among the first line of defense provided by the innate immune system. Macrophages are an established relevant cell model for investigating bacterial pathogen virulence factors, and they are readily set up for high-throughput analysis. In our previous research, libraries of recombinant *Escherichia coli* each carrying end-sequenced *P. asymbiotica* ATCC 43949 genomic fragments (cosmids) were used to identify loci encoding factors cytotoxic to the murine macrophage cell line J774-2 (6). Twenty-three regions of the *P. asymbiotica* genome encoding putative antimacrophage elements were identified from the initial cytotoxicity analysis by using genomic alignment of the end sequences from 88 positive library clones causing >40% reduction in macrophage viability. The minimum genetic region of overlap between two or more clones aligned on the genome is defined as a region of interest (ROI) predicted to express one or more putative antimacrophage effectors.

We used high-content image analysis to quantify the morphological alterations induced in macrophages in response to treatment with preparations from these library clones. Macrophage phenotypes induced by individual clones were quantified by measuring the morphology, staining intensity, and spatial attributes of the cellular cytoskeleton and nuclei. The targets of many pathogen effectors are involved in manipulation of the host cellular and nuclear phenotype, in particular affecting the actin cytoskeleton and the nuclear structure to the advantage of the pathogen. These phenotypes not only relate to previously identified proapoptotic toxins such as Mcf1 (7, 8) but also group new genes into the same phenotype cluster, demonstrating that they may share common aspects of their mode of action. Perhaps more importantly, the approach can identify new groups with currently unknown modes of action.

MATERIALS AND METHODS

Genomic library construction. The *P. asymbiotica* ATCC 43939 cosmid clones used in these experiments were taken from a library constructed using *E. coli* EP1305 containing the pWEB (Epicentre) cosmid vector by MWG Biotech, United Kingdom (4).

Cell culture. The BALB/c monocyte/macrophage cell line J774-2 (from the European Collection of Cell Cultures [ECACC]) was maintained in Dulbecco's modified Eagle's medium (DMEM) supplemented with 10% fetal bovine serum, 5% nonessential amino acids, and 100 μg ml^{-1} ampicillin.

Received 16 October 2013 Accepted 26 November 2013
Published ahead of print 2 December 2013
Address correspondence to Andrea J. Dowling, a.j.dowling@exeter.ac.uk.

doi:10.1128/AEM.03290-13

Macrophage phenotype analysis. Candidate positive cosmid library clones were previously identified in our experiments for their ability to reduce viability by at least 40% compared to untreated macrophages (6). These 88 positive clones were replicated into 96-well microplates containing 100 μl Luria-Bertani medium plus 100 μg ml^{-1} ampicillin. Replicate positive library clone plates were grown for 24 h at 350 rpm and 37°C and subsequently harvested by centrifugation for 10 min at 4,000 rpm. Following centrifugation, 80 μl of the resultant supernatant was aspirated and the bacterial pellet and remaining supernatant were mixed thoroughly with 80 μl of 1 mg ml^{-1} lysozyme in phosphate-buffered saline (PBS) solution. Plates were then incubated at room temperature for a minimum of 1 h, followed by three freeze-thaw cycles before centrifugation at 3,000 rpm for 10 min. Finally, 80 μl of the crude lysate preparations (containing culture supernatant, lysate, and viable library clone *E. coli*) was applied to black 96-well microplates with flat micro-clear bottoms (Greiner Cellstar) containing confluent J774-2 cells arrayed in 96-well plates containing DMEM supplemented with 100 μg ml^{-1} ampicillin. Clone lysates and macrophages were coincubated for 24 h (37°C, 5% CO_2) before medium was aspirated and replaced with phenol red-free DMEM containing an antibiotic cocktail (ampicillin, 100 μg ml^{-1}; gentamicin, 50 μg ml^{-1}; penicillin, 100 U ml^{-1}; streptomycin, 100 μg ml^{-1}; kanamycin, 100 μg ml^{-1}; tetracycline, 5 μg ml^{-1}) and incubated for 2 h (37°C, 5% CO_2) to destroy any remaining live bacteria. Plates were gently washed in sterile 1× PBS before fixing with 4% (wt/vol) paraformaldehyde in PBS for 15 min. Macrophages were permeabilized by being covered with 0.2% Triton X-100 in 1× PBS for 15 min. Staining of the filamentous actin cytoskeleton was carried out with either fluorescein isothiocyanate (FITC)- or tetramethyl rhodamine isothiocyanate (TRITC)-conjugated phalloidin (Sigma), at a 1/500 dilution in 1× PBS at room temperature in the dark for 1 h. Following incubation, microplates were washed 3 times for 5 min each in 1× PBS with the first wash containing 0.12 μg/$μl^{-1}$ Hoechst 33258 (Sigma) to stain nuclei.

Phagocytosis assays. Macrophages arrayed in 96-well plates were preincubated with lysate preparations (as described above) for 1 h before addition of 10 μl of fluorescent yellow-green or fluorescent red amine-modified 1.0-μm polystyrene latex beads (Sigma-Aldrich). Beads were diluted from stock 1 in 100 in sterile PBS before addition. Lysates and beads were then coincubated with the macrophages for 4 h before washing, fixing, and staining (as described above). For phagocytosis assays involving purified Mcf1, macrophages were incubated with 1 μg ml^{-1} for 1 h prior before aspiration of medium and addition of a suspension of 1 mg ml^{-1} pHrodo *E. coli* bioparticles prepared in Hanks balanced salt solution (HBSS), pH 7.5, according to the manufacturer's instructions (Molecular Probes; Invitrogen). The pHrodo bioparticles were incubated with macrophages for 2 h, and fluorescence was measured in a plate reader using excitation of 530 nm and emission of 590 nm. Values represent ±standard errors (SE) of three independent measurements.

High-content image acquisition and analysis. Images of macrophages in 96-well plates were captured using the INCell Analyser 2000 platform (GE Healthcare), using a 40× objective and acquiring nine fields of view per well. Images were analyzed using the INCell Analyser 1000 workstation multitarget analysis module. For macrophage phenotype analysis of image stacks, nuclei were selected using top-hat segmentation and macrophage cells were segmented using multiscale top-hat segmentation; this allows the identification of cellular bodies of various sizes. Multiple nuclear and cellular measures were then acquired from the image stacks for downstream data analysis. For analysis of phagocytosis, an additional detection method to identify and determine the number of intracellular fluorescent latex beads per macrophage was designed. Cell perimeters were defined as previously using multiscale top-hat segmentation; intracellular beads were discriminated using an algorithm to detect inclusions within cell boundaries of a maximum 1.0-μm diameter. Manual inspections were performed throughout to check and validate analyses, ensuring that optimal parameters were set for image processing.

Statistical analysis. Multivariate phenotypic clusters were found using expectation-maximization (EM) algorithms for Gaussian mixture models (9), applied to five cell and nuclear morphology measurements made on each of nine fields of view from 96-well library plates: nuclear area, nuclear intensity, cell area, cell intensity, and cell form factor. This clustering algorithm, applied simply using the mclust library (10) for R 2.12.1 (11), used optimization of the Bayesian information criterion to decide that cell morphologies clustered into five groups. These morphological clusters were of unequal shape, size, and orientation and described five clusters of phenotypic responses to positive cosmid library clones (see Fig. 3). One-way analysis of variance and calculation of least significant difference for phagocytosis assays were carried out using the data analysis Toolpak in Excel.

Toxin purification. Expression and purification of the Mcf1 toxin were carried out as described previously (8).

Insect mortality assays. Last-instar wax moth larvae, *Galleria mellonella*, (Livefoods Direct, United Kingdom), were maintained in the dark at room temperature until use within 5 days of receipt. Frozen 15% glycerol stocks of library clones and wild-type *P. asymbiotica* ATCC 43949 were maintained at −80°C and streaked out onto LB agar (*P. asymbiotica*) or LB agar supplemented with 100 μg ml^{-1} ampicillin (library clones). Plates were incubated at 37°C overnight, and single colonies from the plates were inoculated into LB or LB-ampicillin as appropriate, before incubation at 37°C and 250 rpm overnight. *Galleria* larvae were anesthetized on ice for 15 min prior to injection of 10 μl of bacterial culture using a 100-μl Hamilton syringe into the rear left proleg. Injected *Galleria* larvae were observed and scored for mortality every 24 h for 7 days. Ten insects were injected per treatment, and three replicate experiments were conducted.

RESULTS

Phenotype characterization using high-content microscopy and multivariate analysis. To profile the morphological alterations in macrophages subsequent to treatment with preparations of clones from the 23 ROI, we quantified multiple cellular parameters using high-content image analysis. Multivariate cluster analysis was applied to data obtained for nuclear area, nuclear intensity, cell area, cell intensity, and cell form factor (mean cell roundness index; values range from 1 to infinity where 1 is a perfect circle). This analysis grouped the factors (and controls) into five clusters (Fig. 1A). Three of these groups describe the antimacrophage factors (clusters 2, 3, and 5), and the others describe the untreated controls (cluster 4) and those treated with lysate preparation from the *E. coli* naive library strain (cluster 1). Images for each different cluster type reveal the phenotypic differences between the groups (Fig. 1B). Cluster 1 describes macrophages that have been treated with lysate preparation from control *E. coli*. Both nuclei and cells increase in size; cells have a low form factor, indicating a high degree of cell circularity; and these cells are larger and more rounded than untreated controls, indicating a change in the macrophage phenotype in response to exposure to bacterial components in the *E. coli* preparation. Key features of the cell morphology traits for each cluster are given in Table 1, and the phenotype cluster is listed alongside a description of each ROI in Table 2. Cluster 2 describes nuclear and cytoplasmic condensation and collapse of the actin cytoskeletal structure within treated macrophages. This cluster contains clones from ROI encoding known toxins: Mcf1 toxin, toxin complexes, and XaxAB, along with putative RtxA-like toxins, the Kdp system and putative perforin, and a putative type VI secretion system, all of which have no mode of action described so far in *Photorhabdus*. This classification of ROI with undescribed activity into the same group as known toxins demonstrates that they also have similar effects on host cells and

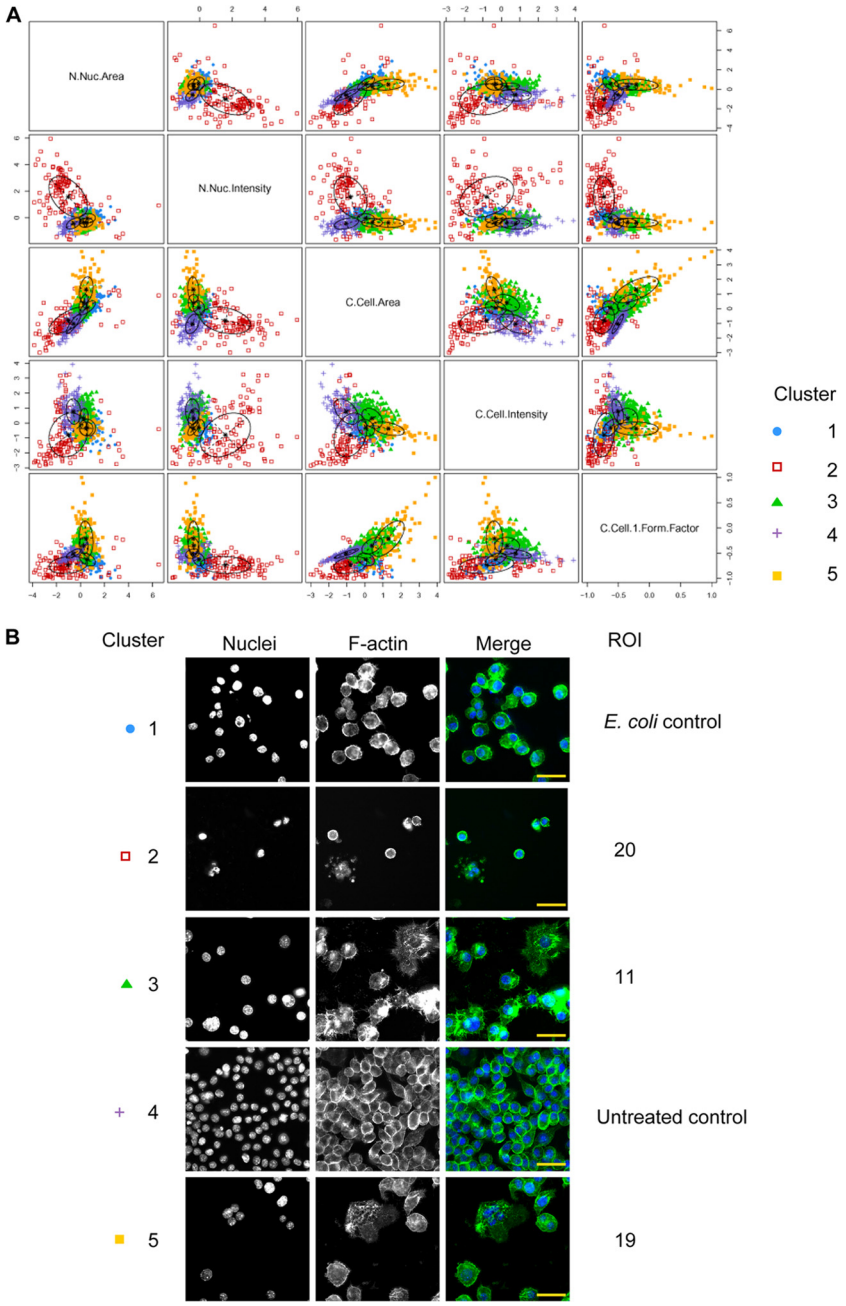

FIG 1 Multivariate cluster analysis of morphometric data from treated macrophages reveals five distinct phenotypic responses. (A) Plot showing clusters in phenotype space for measures of nuclear area, nuclear intensity, cell area, cell intensity, and cell form factor in treated macrophages. Five separate phenotype clusters are isolated. (B) Images representative of key phenotypic features of macrophages falling into the different clusters: cluster 1, typical of the macrophage response seen following treatment with lysate preparation from the control library of *E. coli*; cluster 2, highly condensed, aberrant nuclei and collapsed punctate F-actin cytoskeletal structure with loss of cytoplasmic space and cell-to-cell contact (representative images from ROI 20-treated macrophages); cluster 3, large nuclei and cells with increased formation of protruding cytoskeletal structures (ROI 11); cluster 4, normal morphology of untreated macrophages; cluster 5, very large nuclei and cells with highly altered cellular morphology (ROI 19). Bars, 50 μm.

that the known toxins can act as "phenotypic landmarks." Phenotype cluster 2 represents a group containing known and putative ROI causing an effect on macrophages typical of potent cytolethal toxins; Mcf1 and XaxAB are known proapoptotic toxins (7, 12). Therefore, we hypothesize that cluster 2 represents factors which ultimately induce apoptosis.

Phenotype cluster 3 contains ROI in which the dominant predicted function relates to host cell adhesion and intracellular survival of the pathogen, including adhesins, such as hemagglutinins, and/or nutrient acquisition-related factors. Another key feature within this group is the presence of several predicted secondary metabolite-producing gene clusters. Over a third of the ROI (8 out of 23) contain nonribosomal peptide synthase (NRPS) or polyketide synthase (PKS) clusters, indicating that the small mol-

TABLE 1 Relative cellular characteristics defining each phenotypic cluster[a]

Phenotype cluster	Nuclei	Cells	ROI	Dominant features	Notes
1	Large; high intensity	Large; low form factor	Library *E. coli* control (23)		Response to library *E. coli* lysate preparation
2	Very small; high intensity	Very small; low intensity; low form factor	10, 13, 14, 15, 16, 20, 21, 22, (23)	Toxins	Highly toxic; cell contraction, nuclear condensation, and actin cytoskeletal disintegration
3	Intermediate; low intensity	Intermediate size; intermediate intensity; intermediate form factor	1, 2, 3, 4, 6, 7, 8, 9, (10), 11, 12, 17, 18	PKS/NRPS clusters; hemagglutinins	Cellular distension; cytomodulation
4	Small; low intensity	Small; high intensity; intermediate form factor	Untreated control		Normal macrophage morphology
5	Very large; low intensity	Very large; low intensity; high form factor	19, (6)	CNF1-like (PNF); Ast-like enterotoxin	Multinucleation and cytoskeletal ruffling; cytomodulatory toxins—highly altered cellular morphology

[a] Description of the relative cellular and nuclear characteristics that delineate the different phenotype clusters following multivariate cluster analysis. ROI within the phenotype clusters are given along with the dominant predicted virulence features. ROI in parentheses fall equally into two phenotypic clusters.

ecules that they produce may play an important role in pathogenicity toward macrophages. One of these, ROI 11, contains a yersiniabactin-like PKS cluster. This iron-scavenging siderophore is found in a number of bacterial pathogens (*Yersinia* species, *E. coli*, and plant pathogens) (13, 14). It is required in *Yersinia pestis*, the causative agent of bubonic plague, for persistence within the host and systemic infection (15). Interestingly, a homolog of the maternal adhesion (Mad) fimbrial locus (ROI 2, PAU00182 to PAU00210) also falls into phenotype cluster 3. In the entomopathogen *Photorhabdus luminescens*, this locus is responsible for switching between the pathogenic (insect-killing) and mutualistic (nematode-associated) forms (16). Expression of the locus allows *P. luminescens* to form a mutualistic association by adhering to the nematode intestine and invading and growing within rectal gland cells. This result shows that this analysis is able to reveal bioactive loci with a role not directly related to other pathogen life cycle stages. It is likely that clones expressing ROI 2 are toxic to macrophages due to adhesion by expression of the fimbriae and intracellular growth potentially facilitated by the presence of the SpoT/RelA homolog on this locus.

Intriguingly, only one ROI falls distinctly into cluster 5. Predicted open reading frames within ROI 19 contain homology to a hemagglutinin/hemolysin, a putative insecticidal toxin, and interestingly the predicted "*Photorhabdus* necrosis factor" (PNF), which has homology to the cytotoxic necrotizing factor 1 (CNF1) from uropathogenic *E. coli*. The phenotype data obtained here highlight a unique region with a likely mode of action distinct from the antimacrophage activity seen in response to other ROI. One of the key roles of CNF1, and indeed of many virulence factors, is the modulation of phagocytosis as a strategy to evade the immune system or to exploit the host cell pathways to gain entry and establish intracellular infection (17). Further, almost all uropathogenic *E. coli* strains producing CNF1 also have genes encoding a hemolysin upstream of the toxin (alpha-hemolysin, HlyA), which putatively act together to promote virulence (18).

Phagocytosis modulation screen. Manipulation of the phagocytic pathway to benefit the pathogen is a common infection strategy. Both evasion of phagocytosis and intracellular survival are understood to be part of the *P. asymbiotica* infection cycle (5). In order to begin to relate function to phenotype cluster, we developed and implemented a screen to detect alterations in macrophage phagocytosis resulting from treatment with positive library clone preparations. Eighteen library clones produce effectors capable of significantly increasing mean phagocytosis, and 24 significantly decreased mean phagocytosis following 16 h of coincubation (Fig. 2) (least significant difference [$P = 0.01$] = 0.945). Library clones inhibiting phagocytosis belong to five ROI, 10, 19, 20, 21, and 22; clones promoting phagocytosis belong to five different ROI, 6, 9, 11, 14, and 17. Importantly, the putative pro- or antiphagocytic modulating ROI belong to separate phenotypic clusters, four of the antiphagocytic regions fall into cluster 2, and one falls in cluster 5 (ROI 19). Phenotype cluster 3 is dominant for all prophagocytic regions.

Three examples of factors significantly inhibiting phagocytic activity are found in library clones expressing a type VI secretion system (T6SS) (ROI 21), Mcf1 (ROI 20), and PNF (ROI 19) (Fig. 3). Three examples of factors most significantly promoting macrophage phagocytic activity are found in library clones predicted to encode hemagglutinin/PKS-related (ROI 9), Kdp system/perforin-like (ROI 14), and T6SS-related (ROI 17) regions (Fig. 4). Exposure of macrophages to preparations of library clones containing ROI 14 causes them to dramatically increase their phagocytic activity, and this appears to be the most potent prophagocytic modulator detected from the library screen.

Genetic regions involved in phagocytosis modulation. Detailed genetic maps of the phagocytosis-modulating regions described previously show that they contain either single or multiple effectors (Fig. 5). The prophagocytosis region, ROI 14, contains a Kdp operon encoding a putative high-affinity potassium transporter and two-component activator system. Notably, a predicted perforin-like protein is also encoded by an operon immediately neighboring the Kdp cluster. Perforin-like proteins are pore formers widely expressed by bacterial pathogens, and host cellular response to these cytolytic toxins is regulated by calcium and potassium ion concentrations (19). This region may be involved in macrophage activation resulting in increased phagocytosis and possibly pathogen exit from host cells during the infection cycle. PSI-BLAST analysis reveals that the predicted perforin-like protein contains a membrane attack complex/perforin (MACPF) superfamily conserved domain (E value, 4.29e−09). ROI 9 contains a partial PKS cluster, contact-dependent inhibition (cdi)-related proteins, and filamentous hemagglutinin-like genes plus a hemo-

TABLE 2 Regions of interest: genomic locations, key features, and phenotype cluster[a]

ROI	Locus tag(s)	Key feature(s)	Putative function(s)	PC[b]
1	PAU00135–PAU00155	Serine protease; putative *O*-methyltransferase; iron(II) transport system	Intracellular survival; membrane interaction/degradation	3
2	PAU00182–PAU00210	Permease; fimbria related; ppGp synthetase SpoT/RelA	Adhesion/intracellular survival; Mad fimbrial locus	3
3	PAU00256–PAU00273	Hemolysin proteins PhlA and PhlB; VgrG-like proteins; Pmt1	Virulence factor secretion; putative macrophage toxin	3
4	PAU00428–PAU00441	DNA repair ATPase; type II restriction enzyme	Unknown	1/2
5	PAU00445–PAU00469 (PAU00446–PAU00458 unique region)	Hemagglutinin/hemolysin; PKS	Adhesion, cell lysis, phagosomal/host cell escape; production/secretion of bioactive small molecules	2
6	PAU00764–PAU00803	Phospholipase; Ast enterotoxin; ABC transporter	Toxin production and secretion	3/5
7	PAU00943–PAU00967	Rhs core	Type VI secretion related	3
8	PAU01157–PAU01216 (PAU1194–PAU1201 unique region)	Hemagglutinin-like; *p*-aminobenzoic acid synthase; PE-PGRS family; WD40 repeat protein; PKS cluster; pyocin s2-like protein	Adhesion, cell lysis, phagosomal/host cell escape; biofilm formation/intracellular survival; PE-PGRS; possible type VII secretion; production of bioactive small molecules; bacterial cell death	3
9	PAU01471–PAU01486	SypC-like PKS; putative hemagglutinins	Production/secretion of bioactive molecules; adhesion, cell lysis, phagosomal/host cell escape	3
10	PAU01532–PAU01555	XaxAB; hemagglutinin-like	Proapoptotic toxins; adhesion, cell lysis, phagosomal/host cell escape	2/3
11	PAU02269–PAU02306	Type VI secretion system; filamentous hemagglutinin; yersiniabactin-like PKS	Pathogen multiplication/systemic infection	3
12	PAU02653–PAU02659	Flagellar biosynthesis	Motility/host cell binding	3
13	PAU02667–PAU02675	Pyocin s3 immunity proteins; NRPS/PKS SylA/BylA-like	Production of bioactive small molecules	3
14	PAU02985–PAU03005	Kdp operon; perforin-like; FhaB hemagglutinin	Nutrient acquisition/intracellular survival; pore formation; cell adhesion, colonization	2/3
15	PAU03006–PAU03014	Rhs YD repeat protein	Rhs domain YD repeats	2/3
16	PAU03015–PAU03028	Two RtxA-like toxins; antibiotic PKS; hemagglutinin/hemolysin-like	Toxin/cytotoxicity; production of bioactive small molecules; cell adhesion, colonization, cytotoxicity	2/3
17	PAU03036–PAU03067	Type VI secretion family proteins (ImcF, VgrG, EvpB); PKS	Type VI secretion system; production/secretion of bioactive small molecules	3
18	PAU03306	Filamentous hemagglutinin	Adhesion, cell lysis, phagosomal/host cell escape, cytotoxicity	3
19	PAU03313–PAU03338	Hemagglutinin-like protein; cytotoxic necrotizing factor 1; putative insecticidal toxin	Adhesion, cell lysis, phagosomal/host cell escape; toxins/cytotoxicity	5
20	PAU03356–PAU03369	PKS/NRPS; putative hemagglutinin; Mcf1	Production/secretion of bioactive small molecules; toxin—cytotoxicity	2
21	PAU03792–PAU03828	Type VI-related proteins (ClpA/B, VgrG, ImpA, ImcF)	Type VI secretion system	2
22	PAU03838–PAU03858	Putative peptidase; photopexin AB; insecticidal toxin complexes	Toxins; cytotoxicity	2
23	PAU04258–PAU04306	Multidrug resistance protein; ABC transport related; phage-like proteins	Detoxification; phage related	1/2

[a] Complete inventory of antimacrophage regions of interest from *P. asymbiotica* ATCC 43939. Genomic locations, key gene features within these regions, and putative functions are described.

[b] PC, dominant phenotypic cluster(s) for macrophages treated with clones containing the ROI.

lysin activator (HlyB) which could be involved in processes such as bacterium-host cell attachment, invasion, and colonization. ROI 17 contains a putative T6SS and transcriptional regulator. Predicted T6SS-related proteins are also found in one of the regions with antiphagocytic activity, ROI 21; this region also contains an intracellular multiplication and human macrophage-killing (IcmF) domain protein, but no VgrG-related proteins. ROI 20 contains a putative NRPS cluster, an operon encoding the toxin Mcf1, and also a hemagglutinin and a HecA-like adhesin protein. ROI 19 contains two putative toxins, *Photorhabdus* necrosis factor, which bears homology to CNF1 from *E. coli*, and an insecticidal-toxin-like protein; this region also contains a predicted HecA-like adhesin.

Analysis of effector functions within ROI 20. The majority of the ROI identified contain more than one putative virulence factor, indicating that there may be different antimacrophage activ-

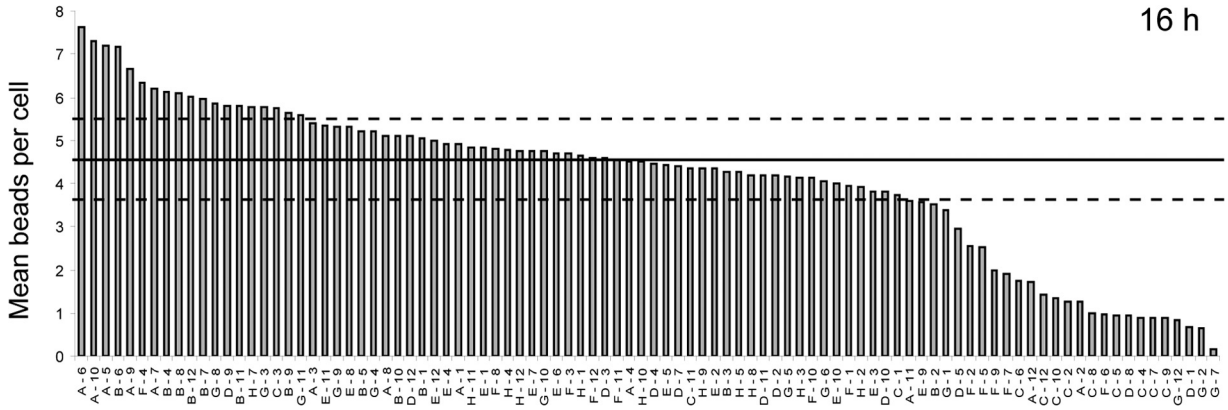

FIG 2 Identification of antimacrophage effectors that modulate phagocytosis. Graph showing the mean number of intracellular green fluorescent latex beads at 16 h. Library clone lysates were preincubated with macrophages for 1 h before application of the bead suspension. The solid line indicates the average number of beads in control macrophages (4.5). Eighteen library clones produced factors capable of significantly increasing mean phagocytosis, and 24 significantly decreased mean phagocytosis following 16 h of coincubation. Upper and lower dashed lines indicate a least significant difference ($P = 0.01$) of 0.945.

ities expressed in the same region. One example of this is ROI 20, which contains a predicted nonribosomal peptide synthase (NRPS) cluster (PAU03356-PAU03357) encoded upstream of an Mcf1 cytotoxin homolog (PAU3369). Clones covering this region are highly cytotoxic to macrophages and group into phenotype cluster 2. Previous characterization of the Mcf1 toxin from the closely related insect pathogen *P. luminescens* revealed it to be a dominant cytotoxin which induces apoptosis in both insect and mammalian cells (7, 8, 20). More recently, Mcf1 has also been demonstrated to rapidly freeze the cytoskeleton of insect phagocytes (21). The NRPS cluster has gene homology to a cluster from *Xenorhabdus nematophila*, the product of which, xenematide, has been described as having weak insecticidal properties against *Galleria mellonella* larvae (22). This genetic region and NRPS cluster are not present in insect-pathogenic *P. luminescens* TT01; the Mcf1 toxin is on a different genetic locus (4). To dissect the function of the NRPS cluster and the *P. asymbiotica* Mcf1 homolog in lysate, preparations were made from clones expressing either the NRPS cluster or Mcf1 alone, and a clone encompassing both the NRPS cluster and Mcf1 (Fig. 6A). Although preparations from clones expressing either the NRPS cluster or Mcf1 are individually toxic to macrophages, the clone encompassing both is more so, with very few macrophages remaining following treatment and those that do showing dramatic cellular and nuclear condensation. Macrophages treated with lysate from the clone expressing the NRPS cluster (clone 1) alone show cellular and nuclear condensation, virtually no cytoplasm remains, and the actin cytoskeleton has collapsed into punctate clusters (Fig. 6B). Clone 2 (NRPS + Mcf1) causes nuclear, cytoplasmic, and cytoskeletal condensation; very few macrophages remain. In clone 3 (Mcf1), few macrophages remain present, these are rounded with granular or condensed actin, and nuclear fragmentation is also evident. To further dissect the potential synergy between Mcf1 and the NRPS product on macrophages, we used purified Mcf1 alone or coincubated with the NRPS product. Macrophages treated for 2 h with 1 $\mu g\ ml^{-1}$ purified Mcf1 toxin display cytoskeletal condensation and granularity, similar to the phenotype seen with macrophages treated with lysate preparation from clone 3 (Mcf1) (Fig. 6C). However, addition of NRPS product following a 30-min preincubation with Mcf1 caused a dramatic alteration of the cytoskeleton causing the formation of large "tangled" actin protrusions and ruffles. Preincubation of macrophages with NRPS product and subsequent addition of purified Mcf1 reproduced the effect. Macrophages coincubated with Mcf1 and an NRPS product from a separate region of interest (ROI 9) did not show this dramatic alteration in cytoskeletal structure, and macrophages appeared like those treated with Mcf1 alone. Insect mortality assays also demonstrate that the clone encompassing both Mcf1 and the NRPS cluster (clone 2) is considerably more toxic to *Galleria mellonella* than are clones expressing Mcf1 or the NRPS cluster alone (Fig. 6D). All *Galleria* insects injected with clone 2 are dead 72 h after treatment, compared to 47% of those injected with clone 3 (Mcf1) alone and 13% of those injected with clone 1 (NRPS). Comparison of *Galleria* phenotypes 72 h postinjection reveals heavy phenotypic blackening in those injected with clone 2 (NRPS + Mcf1); this is also apparent in the majority of insects injected with clone 3 (Mcf1) (Fig. 6E). Conversely, in *Galleria* insects injected with clone 1 (NRPS), a number develop a pink-gray coloration and reduced locomotion; these go on to die over the course of the experiment.

ROI 20 falls into phenotype cluster 2 and has an antiphagocytic effect on macrophages. We investigated whether the Mcf1 toxin within ROI 20 was responsible for this inhibition of phagocytosis. Macrophages pretreated with 1 $\mu g\ ml^{-1}$ purified Mcf1 toxin fail to internalize green fluorescent latex beads (Fig. 7A). Quantification of phagocytosis shows that Mcf1 is capable of reducing levels of phagocytosis by almost 70% compared to untreated macrophages (Fig. 7B).

DISCUSSION

Application of statistical analysis to multiple cellular measures obtained from macrophages treated with library clones expressing putative bacterial effectors reveals that we can group macrophage response based on phenotype. We reveal five phenotype clusters: clusters 1 and 4 describe control naive *E. coli* lysate-treated macrophages and untreated macrophages, respectively, and clusters 2, 3, and 5 describe significantly different cell morphology phenotypes displayed by treated macrophages which relate to putative effector function.

Modulation of phagocytosis is one of the key factors in the

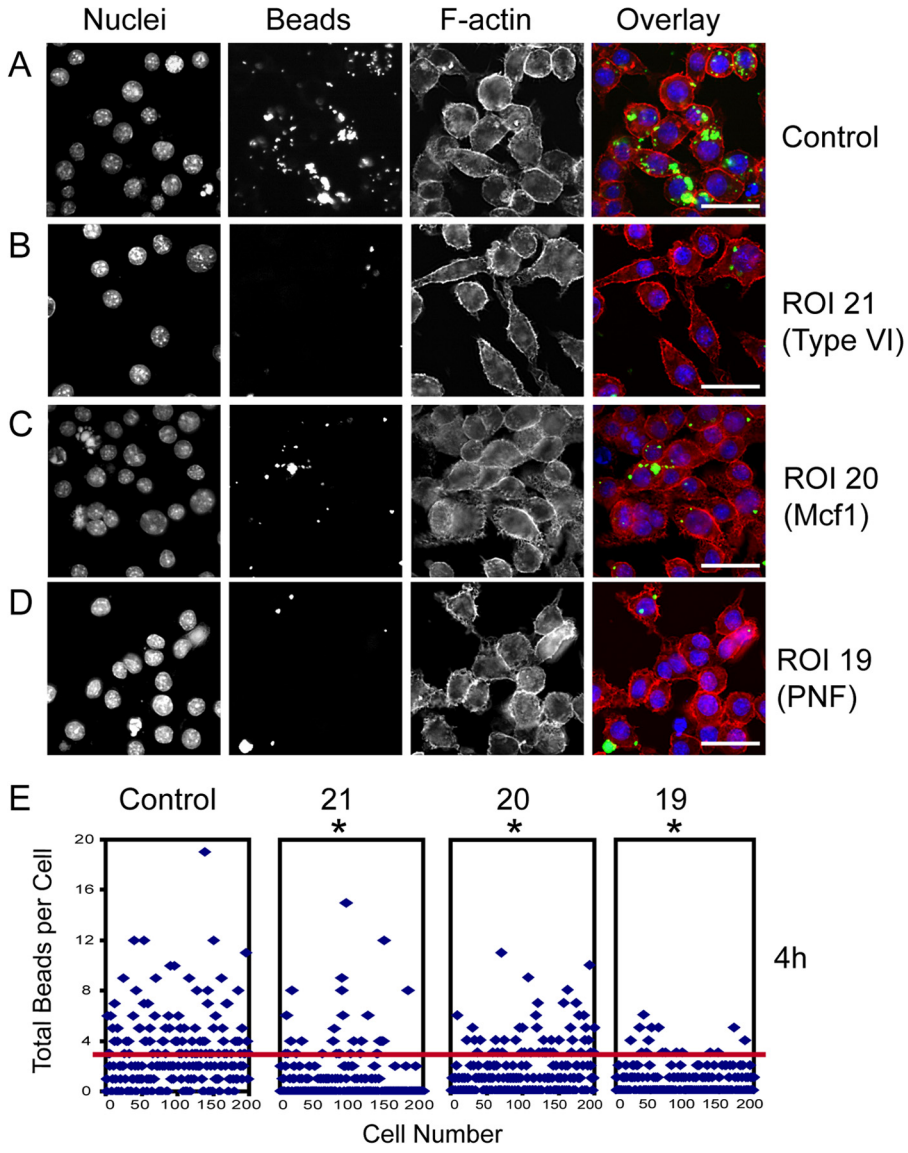

FIG 3 Antiphagocytic activity caused by clones encoding toxin-like genes and type VI-related proteins. (A to D) Macrophages treated with lysate from vector-only *E. coli* control (A) and those treated with clones expressing ROI 21 type VI-related proteins (B), ROI 20 *P. asymbiotica* Mcf1 homolog (C), and ROI 19 CNF1-related toxin (D), for 1 h before addition of fluorescein-labeled latex beads followed by a 3-h coincubation. Macrophage F-actin cytoskeletal structures are stained with TRITC-conjugated phalloidin (red), intracellular beads are shown in green, and nuclei are stained with Hoechst 33258 (blue). Bars, 10 μm. (E) Scatter plots showing total intracellular beads per cell at 4 h versus cell number for control, type VI (ROI 21), Mcf1 (ROI 20), and CNF1-like lysate-treated macrophages (ROI 19). The red line shows the average number of beads per macrophage in the untreated control. The asterisk indicates statistical significance versus control as determined by Student's *t* test ($P < 0.01$).

establishment of successful infection by a pathogen (23). In order to link functional characteristics to the phenotype clusters, we developed a phagocytosis screen to look for factors among the 23 antimacrophage ROI with the ability to promote or inhibit phagocytosis. Phenotype clusters 2 and 5 contained ROI with antiphagocytic effects, and phenotype cluster 3 contained ROI with prophagocytic effects. Treatments with preparations from clones containing PNF (ROI 19, phenotype cluster 5) caused highly significant inhibition of phagocytosis. CNF1 has previously been observed to inhibit phagocytosis in professional phagocytes (17, 24). Interestingly, both pro- and antiphagocytic activities were linked with type VI secretion-related ROI. Although impairment of phagocytosis by a *Vibrio cholerae* type VI secretion system has been described elsewhere (25), we believe that this is the first time that involvement of type VI-related proteins in the promotion of phagocytosis has been suggested. The most dramatic and significant increase in phagocytosis is linked to ROI 14. ROI 14 is highly toxic over 16 h; however, it potently increases phagocytosis with effects visible at 4 h following coincubation. This ROI encodes a Kdp system and a MACPF-domain perforin-like protein (PAU02991). The Kdp system was originally identified in *E. coli* K-12 as a high-affinity ATP-driven transport system for the uptake of potassium ions composed of the KdpABC operon, which encodes three membrane subunits, and the KdpDE two-component regulatory system (26–29). The Kdp system from *P. asymbiotica* has an implied role in intracellular survival in invertebrate

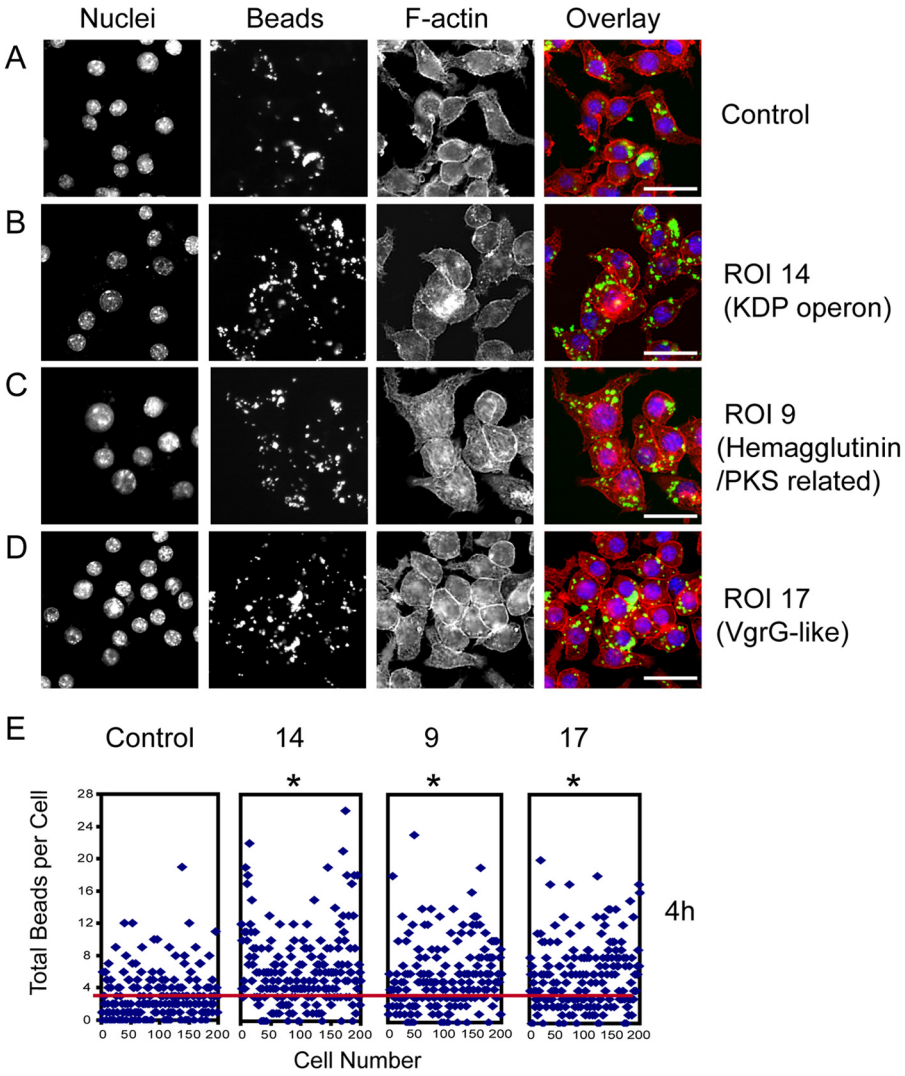

FIG 4 Prophagocytic activity resulting from clones encoding a Kdp potassium transporter system and hemagglutinin-related and VgrG-like proteins. (A to D) Macrophages treated with lysate from vector-only *E. coli* control (A) and treated with clones expressing ROI 14 containing a Kdp potassium transporter (B), ROI 9 hemagglutinin and PKS-like protein (C), and ROI 17 VgrG-related proteins (D). Macrophages were preincubated with lysates for 1 h before addition of fluorescein-labeled latex beads for a 3-h coincubation. Macrophage F-actin cytoskeletal structures are stained with TRITC-conjugated phalloidin (red), intracellular beads are shown in green, and nuclei are stained with Hoechst 33258 (blue). Bars, 10 μm. (E) Scatter plots showing total intracellular beads per cell at 4 h versus cell number for control, Kdp (ROI 14) hemagglutinin/PKS (ROI 9), and VgrG-like (ROI 17) lysate-treated macrophages. The red line shows the average number of beads per macrophage in the untreated control. The asterisk indicates statistical significance versus control as determined by Student's *t* test ($P < 0.01$).

phagocytes (30). Intriguingly, deletion of KdpDE in *Mycobacterium tuberculosis* causes an increase in virulence and has therefore been suggested to play a role in regulating the growth of the pathogen *in vivo* (31). Also, recently, a Kdp operon from *Staphylococcus aureus* has been observed to act as a global virulence factor regulator, rather than acting as a major potassium ion transporter (32). Directly adjacent to the Kdp system in *P. asymbiotica* is a perforin-like protein (PAU02991). Perforin-like cytolytic proteins (pore-forming toxins) are expressed by many bacterial pathogens (19). A homolog of PAU02991 was recently identified in *P. luminescens* TT01, Plu-MACPF (PLU1415), and the crystal structure was resolved (33). This study demonstrated that the MACPF domain has structural similarity to the pore-forming cholesterol-dependent cytolysins (CDCs) from Gram-positive bacteria, suggesting that MACPF proteins and CDCs may share a lytic mechanism. However, no lytic activity was observed using purified Plu-MACPF, and it was believed that some form of cofactor may be required (33). Notably, Plu-MACPF is also a direct neighbor to a Kdp system in *P. luminescens* TT01 as is PAU02991 in ROI 14 identified in *P. asymbiotica*. Potassium (along with calcium) is considered to be the key regulator of cellular response to pore formation. The cytosolic drop normally associated with pore-forming activity is associated with a number of effects, including autophagy, translational arrest, and the activation of mitogen-activated protein (MAP) kinase pathways and proteolytic cascades (19). Potassium concentration is also important in the killing of engulfed pathogens in the phagolysosome. Recently, a perforin-like protein from the parasitic protozoan *Toxoplasma gondii* has been shown to fa-

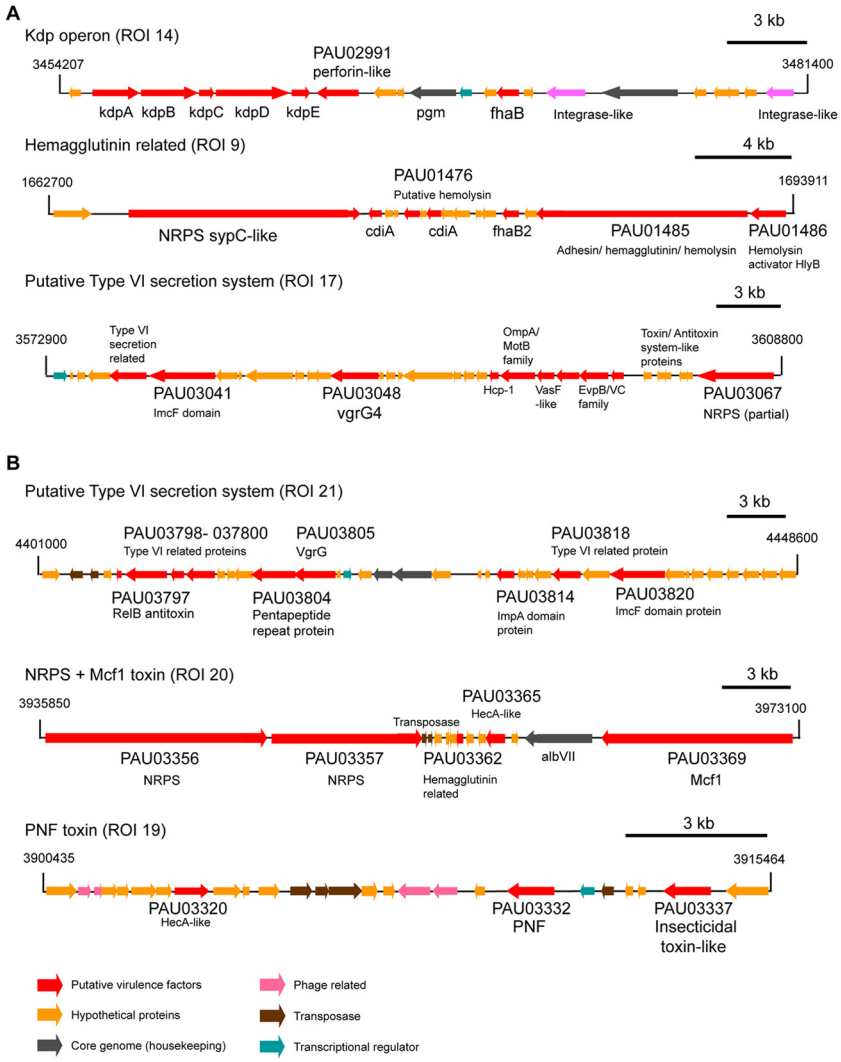

FIG 5 Detailed genetic maps of six putative phagocytosis-modulating regions. Genomic organization of six antimacrophage loci isolated by the screen that positively (A) and negatively (B) modulate macrophage phagocytosis. Genes putatively involved in antimacrophage activity and phagocytosis modulation are highlighted in red. The roles of the remaining genes in the region are provided in the color key based on the original genome annotation and BLASTX analysis of the ROI.

cilitate exit from host cells, implying a role in dissemination of infection (34). It is possible that the putative effectors in this ROI may play a role in the intracellular life cycle stage of *P. asymbiotica* by promoting internalization of the pathogen as well as equipping it with the ability to survive within the cell, and possibly contributing to dissemination. Our data suggest that there are several factors capable of promoting or limiting phagocytosis by macrophages, and these may play a role in different stages of *P. asymbiotica* infection processes.

The majority of the ROI detected contain more than one putative effector. ROI 20 is highly toxic to macrophages, falls into phenotype cluster 2, and is antiphagocytic; it contains not only an Mcf1 toxin homolog but also an NRPS cluster. First assumptions relating to previous research would suggest that Mcf1 toxin alone is capable of causing high cytotoxicity levels in macrophages (7, 20), raising the question as to why the NRPS cluster is also present in ROI 20. Detailed dissection of ROI 20 revealed that clones expressing either Mcf1 or the NRPS cluster were individually cytotoxic to macrophages; however, a clone expressing both was more cytotoxic. Further, *Galleria mellonella* insects injected with a clone expressing both the NRPS cluster and Mcf1 suffered higher rates of mortality than did those injected with clones expressing the NRPS cluster or Mcf1 individually. To explore this potential synergicinteraction between Mcf1 and the NRPS product, we carried out early time point studies to look at events upstream of macrophage cell or whole-insect death. Macrophages treated with both the NRPS product and purified Mcf1 revealed dramatic alterations to the cytoskeleton with the formation of large tangled actin filament protrusions and ruffles. This phenotype is much in contrast to the granular, condensed cytoskeleton seen in response to Mcf1 treatment alone. Mcf1 has been previously documented as "freezing" the cytoskeleton of insect phagocytes (21). This frozen cytoskeleton resulting from Mcf1 treatment can, however, be dramatically altered or possibly "unlocked" by adding lysate preparation from a clone expressing the neighboring NRPS cluster upstream of Mcf1. Prior incubation with NRPS product and

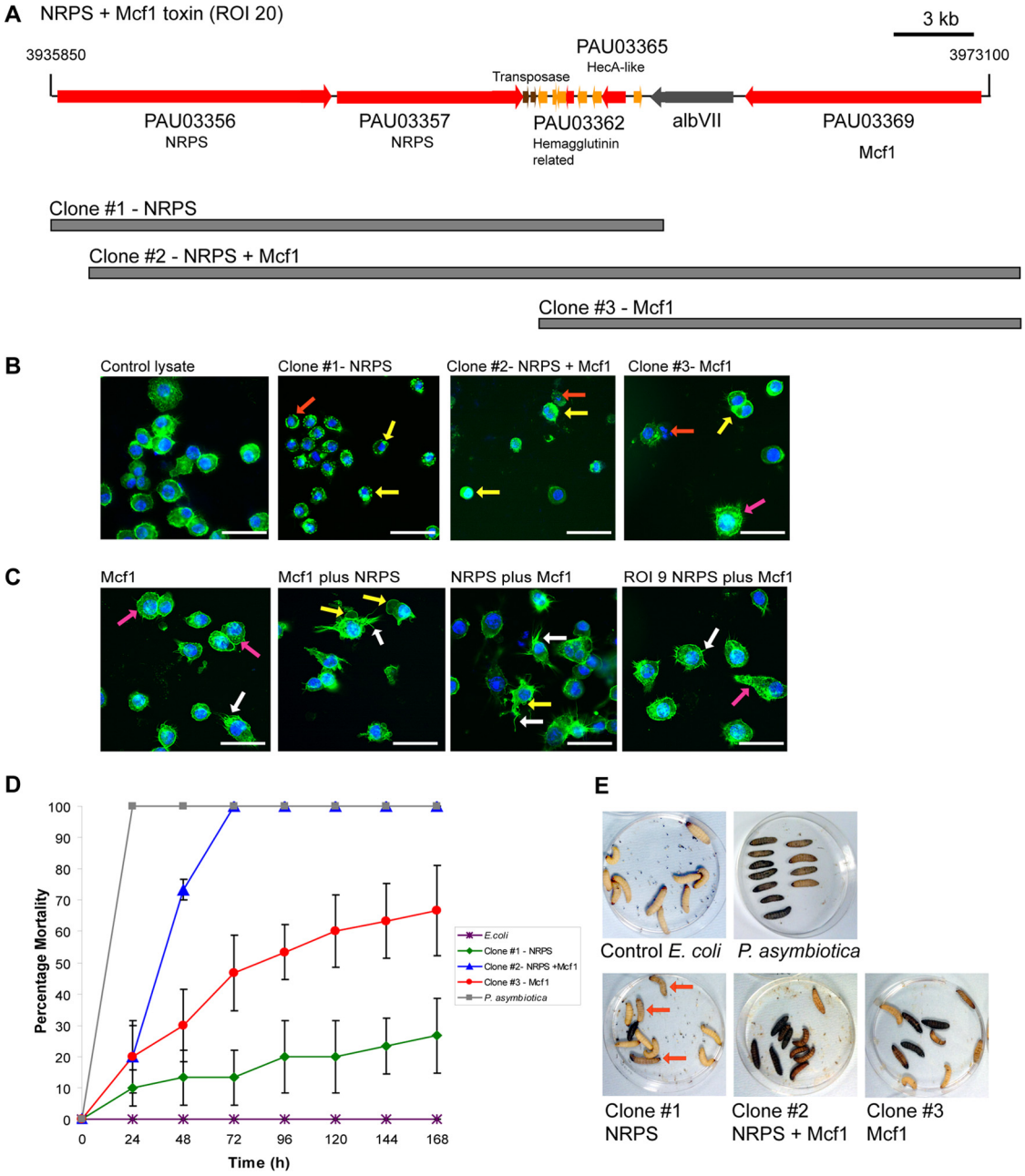

FIG 6 Toxicity of Mcf1 is enhanced by a neighboring NRPS cluster. (A) Open reading frame map showing the predicted genes within ROI 20. PAU03356 and PAU03357 encode a predicted NRPS cluster neighboring the Mcf1 toxin homolog PAU03369. Underneath the open reading frame map, the coverage of clones used to dissect activity within this region is depicted. Clone 1 contains the NRPS cluster, clone 2 spans the NRPS cluster and the Mcf1 toxin, and clone 3 contains the Mcf1 toxin. (B) Effects on macrophage nuclear and cytoskeletal morphology following 4 h of incubation with lysate preparations: from left to right, control library strain *E. coli*, clone 1 (NRPS), clone 2 (spanning NRPS and Mcf1), and clone 3 (Mcf1). Clone 1 (NRPS) causes nuclear shrinkage and fragmentation (red arrow) and collapse of the actin cytoskeleton into a punctate form surrounding the nucleus (yellow arrows). Clone 2 (NRPS + Mcf1) causes nuclear (red arrow) and cytoplasmic and cytoskeletal (yellow arrows) condensation; very few macrophages remain. In clone 3 (Mcf1), few macrophages remain; these are rounded with condensed actin (yellow arrow) or granular actin (pink arrow); nuclear fragmentation is also evident (red arrow). (C) Coincubation analysis with purified Mcf1 and NRPS clone lysate preparation. The leftmost panel shows the phenotype of macrophages incubated with 1 μg ml^{-1} pure Mcf1 toxin for 1 h 30 min, showing granular cytoskeletal staining (pink arrows). The Mcf1-plus-NRPS panel shows the effect on macrophages preincubated with pure Mcf1 for 30 min prior to addition of NRPS lysate and subsequent coincubation for 60 min. The NRPS-plus-Mcf1 panel shows the inverse of this treatment, with macrophages preincubated with NRPS lysate for 30 min prior to addition of purified Mcf1 and coincubation for 60 min. In both cases, macrophages show the formation of dramatic cytoskeletal protrusions in the form of "tangled" filaments (white arrows) or ruffles (yellow arrows). The far right panel shows the coincubation of Mcf1 with a lysate preparation from a library clone expressing a nonneighbor NRPS (ROI 9); the macrophage phenotype is like the phenotype of those treated with Mcf1 alone. (D) *Galleria mellonella* mortality assay. Clone 2 (NRPS + Mcf1) rapidly causes high levels of mortality—100% of insects are dead at 72 h postinjection—whereas clone 3 (Mcf1 only) causes ~50% mortality at this time point. Clone 1 (NRPS only) shows weak insecticidal activity. Control injections of wild-type *P. asymbiotica* ATCC 43949 kill 100% of *Galleria* insects within 24 h. *Galleria* insects injected with control *E. coli* show no mortality. (E) Images of *Galleria mellonella* larvae 72 h postinjection. The top panels show that *Galleria* insects injected with control *E. coli* are cream colored and healthy in comparison to those injected with *P. asymbiotica*, which are all heavily melanized and dead. The lower panels (from left to right) show *Galleria* insects injected with clones 1 (NRPS), 2 (NRPS + Mcf1), and 3 (Mcf1). Of insects injected with clone 1, the heavily melanized larvae are dead and three are slightly melanized, are brown/pink in color, and show further symptoms of toxicity via reduced locomotion in comparison to control *E. coli*. Of *Galleria* insects injected with clone 2 (NRPS + Mcf1), all are heavily melanized and dead. Of *Galleria* insects injected with clone 3 (Mcf1), the majority are melanized and five are dead.

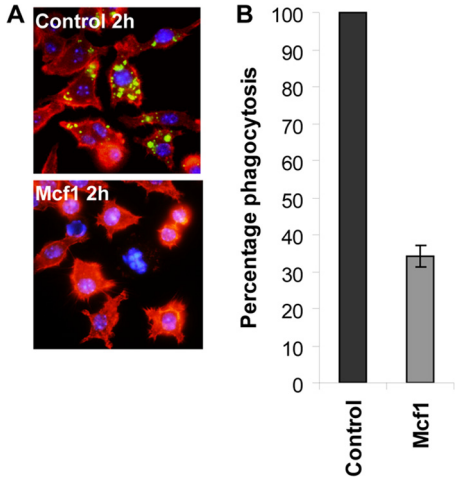

FIG 7 Purified Mcf1 toxin reduces phagocytosis. (A) J774 macrophages were coincubated with FITC-labeled latex beads for 2 h. The top panel shows control cells which have internalized beads. The lower panel shows macrophages pretreated with 1 μg ml^{-1} purified Mcf1 for 30 min prior to addition of the bead suspension; no beads are visible within the macrophages. (B) Quantitative analysis of phagocytosis inhibition by Mcf1. The graph shows percent phagocytosis of pHrodo bioparticles by macrophages preincubated with Mcf1 for 30 min. Mcf1 reduces phagocytosis to 34% (SE, ±2.88) in comparison to untreated macrophages.

subsequent treatment with Mcf1 also produce the same cytoskeletal phenotype. Together, these data are suggestive of synergism between a putative secondary metabolite encoded by the NRPS cluster and Mcf1 toxin. Although they are well studied as virulence factors in fungi, relatively little is known about the role of secondary metabolites in bacterial pathogenicity. Such a synergy, or interaction, of secondary metabolites with toxins or other effectors has not previously been documented to our knowledge. However, synergistic interactions of effectors at distal sites may be missed as this methodology looks only at the products expressed from the 40 kb of DNA in individual library cosmids.

The ability to carry out high-content analysis and imaging in multiwell plates allows us to investigate numerous individual factors simultaneously while applying identical criteria. This high-throughput methodology facilitates the rapid morphological phenotype profiling of eukaryotic cells in response to treatment with recombinant pathogen library clones. This technique provides us with a shortlist of target genes and genetic regions for further analysis.

Future analysis methods can be developed to further narrow down function within phenotype clusters by visualization and quantification of measurements relating to the status of subcellular targets, e.g., organelles (in particular the Golgi apparatus and mitochondria), proteins, or even metal trafficking (potassium/calcium ions, e.g., Kdp). Further infection-relevant analysis for adhesion, macrophage activation, intracellular survival and persistence, and mode of cell death (induction of apoptosis/necrosis) will link these infection mechanisms with candidate effector genes. These methods not only are applicable to bacterial pathogens but have the potential to be developed and directed toward the classification of candidate effectors from any pathogen genome for which a genomic library can be made. However, we acknowledge that *P. asymbiotica* is a member of the *Enterobacteriaceae* and thus expression of DNA from this pathogen in *E. coli* vectors is relatively straightforward. Expression of more distantly related genomic DNA may be poor in *E. coli* and lead to false-negative results. Optimization of the methodology may be required to improve expression by, for example, using hosts beyond *E. coli* such as nonpathogenic Gram-positive bacteria (e.g., *Bacillus subtilis*) or yeast.

ACKNOWLEDGMENTS

We thank P. Wilkinson for bioinformatic advice and discussion and R. Ffrench-Constant for reviewing the manuscript.

The authors have declared that no competing interests exist.

This work was supported by the BBSRC (www.bbsrc.ac.uk) (BB/E021328/1). The funders had no role in study design, data collection and analysis, decision to publish, or preparation of the manuscript.

REFERENCES

1. **Zimmer C.** 2012. From microbes to numbers: extracting meaningful quantities from images. Cell. Microbiol. **14:**1828–1835. http://dx.doi.org/10.1111/cmi.12032.
2. **Forst S, Dowds B, Boemare N, Stackebrandt E.** 1997. Xenorhabdus and Photorhabdus spp.: bugs that kill bugs. Annu. Rev. Microbiol. **51:**47–72. http://dx.doi.org/10.1146/annurev.micro.51.1.47.
3. **Gerrard J, Waterfield N, Vohra R, Ffrench-Constant R.** 2004. Human infection with Photorhabdus asymbiotica: an emerging bacterial pathogen. Microbes Infect. **6:**229–237. http://dx.doi.org/10.1016/j.micinf.2003.10.018.
4. **Wilkinson P, Waterfield NR, Crossman L, Corton C, Sanchez-Contreras M, Vlisidou I, Barron A, Bignell A, Clark L, Ormond D, Mayho M, Bason N, Smith F, Simmonds M, Churcher C, Harris D, Thompson NR, Quail M, Parkhill J, Ffrench-Constant RH.** 2009. Comparative genomics of the emerging human pathogen Photorhabdus asymbiotica with the insect pathogen Photorhabdus luminescens. BMC Genomics **10:**302. http://dx.doi.org/10.1186/1471-2164-10-302.
5. **Costa SC, Girard PA, Brehelin M, Zumbihl R.** 2009. The emerging human pathogen Photorhabdus asymbiotica is a facultative intracellular bacterium and induces apoptosis of macrophage-like cells. Infect. Immun. **77:**1022–1030. http://dx.doi.org/10.1128/IAI.01064-08.
6. **Waterfield NR, Sanchez-Contreras M, Eleftherianos I, Dowling A, Yang G, Wilkinson P, Parkhill J, Thomson N, Reynolds SE, Bode HB, Dorus S, Ffrench-Constant RH.** 2008. Rapid virulence annotation (RVA): identification of virulence factors using a bacterial genome library and multiple invertebrate hosts. Proc. Natl. Acad. Sci. U. S. A. **105:**15967–15972. http://dx.doi.org/10.1073/pnas.0711114105.
7. **Dowling AJ, Daborn PJ, Waterfield NR, Wang P, Streuli CH, Ffrench-Constant RH.** 2004. The insecticidal toxin Makes caterpillars floppy (Mcf) promotes apoptosis in mammalian cells. Cell. Microbiol. **6:**345–353. http://dx.doi.org/10.1046/j.1462-5822.2003.00357.x.
8. **Dowling AJ, Waterfield NR, Hares MC, Le Goff G, Streuli CH, Ffrench-Constant RH.** 2007. The Mcf1 toxin induces apoptosis via the mitochondrial pathway and apoptosis is attenuated by mutation of the BH3-like domain. Cell. Microbiol. **9:**2470–2484. http://dx.doi.org/10.1111/j.1462-5822.2007.00974.x.
9. **Fraley C, Raftery AE.** 2002. Model-based clustering, discriminant analysis, and density estimation. J. Am. Stat. Assoc. **97:**611–631. http://dx.doi.org/10.1198/016214502760047131.
10. **Fraley C, Raftery AE, Murphy TB, Scrucca L.** 2012. mclust version 4 for R: normal mixture modeling for model-based clustering, classification, and density estimation. Technical report no. 597. Department of Statistics, University of Washington, Seattle, WA.
11. **R Development Core Team.** 2012. R: a language and environment for statistical computing. R Development Core Team, Vienna, Austria.
12. **Vigneux F, Zumbihl R, Jubelin G, Ribeiro C, Poncet J, Baghdiguian S, Givaudan A, Brehelin M.** 2007. The xaxAB genes encoding a new apoptotic toxin from the insect pathogen Xenorhabdus nematophila are present in plant and human pathogens. J. Biol. Chem. **282:**9571–9580. http://dx.doi.org/10.1074/jbc.M604301200.
13. **Bach S, de Almeida A, Carniel E.** 2000. The Yersinia high-pathogenicity island is present in different members of the family Enterobacteriaceae. FEMS Microbiol. Lett. **183:**289–294. http://dx.doi.org/10.1111/j.1574-6968.2000.tb08973.x.

14. **Schubert S, Rakin A, Karch H, Carniel E, Heesemann J.** 1998. Prevalence of the "high-pathogenicity island" of Yersinia species among Escherichia coli strains that are pathogenic to humans. Infect. Immun. **66:**480–485.
15. **Bearden SW, Fetherston JD, Perry RD.** 1997. Genetic organization of the yersiniabactin biosynthetic region and construction of avirulent mutants in Yersinia pestis. Infect. Immun. **65:**1659–1668.
16. **Somvanshi VS, Sloup RE, Crawford JM, Martin AR, Heidt AJ, Kim KS, Clardy J, Ciche TA.** 2012. A single promoter inversion switches Photorhabdus between pathogenic and mutualistic states. Science **337:**88–93. http://dx.doi.org/10.1126/science.1216641.
17. **Capo C, Meconi S, Sanguedolce MV, Bardin N, Flatau G, Boquet P, Mege JL.** 1998. Effect of cytotoxic necrotizing factor-1 on actin cytoskeleton in human monocytes: role in the regulation of integrin-dependent phagocytosis. J. Immunol. **161:**4301–4308.
18. **Garcia TA, Ventura CL, Smith MA, Merrell DS, O'Brien AD.** 2013. Cytotoxic necrotizing factor 1 and hemolysin from uropathogenic Escherichia coli elicit different host responses in the murine bladder. Infect. Immun. **81:**99–109. http://dx.doi.org/10.1128/IAI.00605-12.
19. **Bischofberger M, Iacovache I, van der Goot FG.** 2012. Pathogenic pore-forming proteins: function and host response. Cell Host Microbe **12:**266–275. http://dx.doi.org/10.1016/j.chom.2012.08.005.
20. **Daborn PJ, Waterfield N, Silva CP, Au CP, Sharma S, Ffrench-Constant RH.** 2002. A single Photorhabdus gene, makes caterpillars floppy (mcf), allows Escherichia coli to persist within and kill insects. Proc. Natl. Acad. Sci. U. S. A. **99:**10742–10747. http://dx.doi.org/10.1073/pnas.102068099.
21. **Vlisidou I, Dowling AJ, Evans IR, Waterfield N, Ffrench-Constant RH, Wood W.** 2009. Drosophila embryos as model systems for monitoring bacterial infection in real time. PLoS Pathog. **5:**e1000518. http://dx.doi.org/10.1371/journal.ppat.1000518.
22. **Lang G, Kalvelage T, Peters A, Wiese J, Imhoff JF.** 2008. Linear and cyclic peptides from the entomopathogenic bacterium Xenorhabdus nematophilus. J. Nat. Prod. **71:**1074–1077. http://dx.doi.org/10.1021/np800053n.
23. **Sarantis H, Grinstein S.** 2012. Subversion of phagocytosis for pathogen survival. Cell Host Microbe **12:**419–431. http://dx.doi.org/10.1016/j.chom.2012.09.001.
24. **Hofman P, Le Negrate G, Mograbi B, Hofman V, Brest P, Alliana-Schmid A, Flatau G, Boquet P, Rossi B.** 2000. Escherichia coli cytotoxic necrotizing factor-1 (CNF-1) increases the adherence to epithelia and the oxidative burst of human polymorphonuclear leukocytes but decreases bacteria phagocytosis. J. Leukoc. Biol. **68:**522–528.
25. **Ma AT, Mekalanos JJ.** 2010. In vivo actin cross-linking induced by Vibrio cholerae type VI secretion system is associated with intestinal inflammation. Proc. Natl. Acad. Sci. U. S. A. **107:**4365–4370. http://dx.doi.org/10.1073/pnas.0915156107.
26. **Laimins LA, Rhoads DB, Epstein W.** 1981. Osmotic control of kdp operon expression in Escherichia coli. Proc. Natl. Acad. Sci. U. S. A. **78:**464–468. http://dx.doi.org/10.1073/pnas.78.1.464.
27. **Polarek JW, Williams G, Epstein W.** 1992. The products of the kdpDE operon are required for expression of the Kdp ATPase of Escherichia coli. J. Bacteriol. **174:**2145–2151.
28. **Rhoads DB, Waters FB, Epstein W.** 1976. Cation transport in Escherichia coli. VIII. Potassium transport mutants. J. Gen. Physiol. **67:**325–341.
29. **Walderhaug MO, Polarek JW, Voelkner P, Daniel JM, Hesse JE, Altendorf K, Epstein W.** 1992. KdpD and KdpE, proteins that control expression of the kdpABC operon, are members of the two-component sensor-effector class of regulators. J. Bacteriol. **174:**2152–2159.
30. **Vlisidou I, Eleftherianos I, Dorus S, Yang G, Ffrench-Constant RH, Reynolds SE, Waterfield NR.** 2010. The KdpD/KdpE two-component system of Photorhabdus asymbiotica promotes bacterial survival within M. sexta hemocytes. J. Invertebr. Pathol. **105:**352–362. http://dx.doi.org/10.1016/j.jip.2010.09.020.
31. **Parish T, Smith DA, Kendall S, Casali N, Bancroft GJ, Stoker NG.** 2003. Deletion of two-component regulatory systems increases the virulence of Mycobacterium tuberculosis. Infect. Immun. **71:**1134–1140. http://dx.doi.org/10.1128/IAI.71.3.1134-1140.2003.
32. **Xue T, You Y, Hong D, Sun H, Sun B.** 2011. The Staphylococcus aureus KdpDE two-component system couples extracellular K+ sensing and Agr signaling to infection programming. Infect. Immun. **79:**2154–2167. http://dx.doi.org/10.1128/IAI.01180-10.
33. **Rosado CJ, Buckle AM, Law RH, Butcher RE, Kan WT, Bird CH, Ung K, Browne KA, Baran K, Bashtannyk-Puhalovich TA, Faux NG, Wong W, Porter CJ, Pike RN, Ellisdon AM, Pearce MC, Bottomley SP, Emsley J, Smith AI, Rossjohn J, Hartland EL, Voskoboinik I, Trapani JA, Bird PI, Dunstone MA, Whisstock JC.** 2007. A common fold mediates vertebrate defense and bacterial attack. Science **317:**1548–1551. http://dx.doi.org/10.1126/science.1144706.
34. **Kafsack BF, Pena JD, Coppens I, Ravindran S, Boothroyd JC, Carruthers VB.** 2009. Rapid membrane disruption by a perforin-like protein facilitates parasite exit from host cells. Science **323:**530–533. http://dx.doi.org/10.1126/science.1165740.